The Laser-Doppler-Velocimeter (LDV) used in the ISL shock tunnel for nozzle flow velocity diagnostics

F. Seiler and A. George

French-German Research Institute of Saint-Louis (ISL)
5 Rue du Général Cassagnou, F-68301 Saint-Louis, France

Abstract

The ISL shock tubes, see Patz (1970, 1971), were used for several years with square nozzles as shock tunnels for expanding the shock tube flow to hypersonic flow speeds. For this purpose the circular shock tube cross section contour is transformed by means of a specially designed insert from circular to a rectangular nozzle shape, influencing the homogeneity of the circular shock tube flow at the beginning of the nozzle. Furthermore, the flow in this divergent duct is distorted by the boundary layers developing at the nozzle walls. At each of the four corners, formed by two nozzle walls, the wall boundary layers overlap, resulting in a corner boundary layer. The disadvantage of inhomogeneous flow development at the beginning of the square nozzle and the additional distortion by the edge boundary layers was overcome by using circular nozzles attached at the end of the shock tube facility. In this case the circular shock tube contour is continued into the inner of the nozzle. This conical nozzle is used in the non-reflected mode for accelerating directly the supersonic shock tube flow, see chapter 2. A principle sketch of the shock tunnel facility, operated with a non-reflected nozzle, is given in Fig. 1 with the high-pressure driver tube and the lower pressure driven tube containing the test gas.

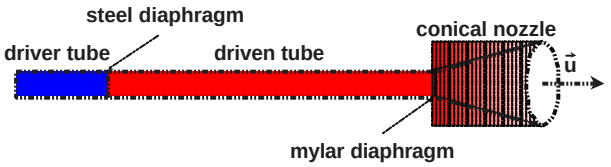

Fig. 1. Principle sketch of shock tunnel facility

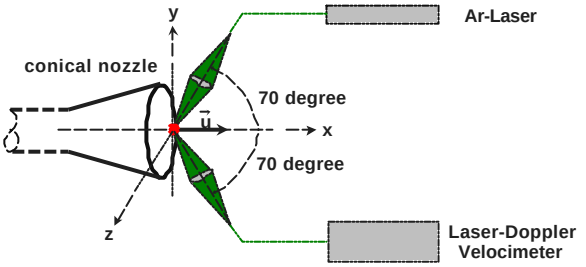

Fig. 2. Optical arrangement of LDV Measurement

In order to get information on the quality of the flow produced by flow expansion inside of the nozzle, velocity measurements have been performed at the nozzle exit using the Laser-Doppler-Velocimeter (LDV) developed by Smeets and George (1978) at ISL. With this device the velocity of tracer particles seeded into the flow was analysed by detecting the Doppler shift $d\nu$ of the light scattered by the tracer particles passing the measuring volume while being illuminated by a laser light source, here an Ar^+-laser, see Fig. 2. The LDV-System uses a Michelson-Interferometer for transforming the Doppler frequency shift $d\nu$ into a varying light intensity output dI. This light intensity variation dI is continuous and proportional to the frequency shift $d\nu$. In coupling $d\nu$ with the Doppler effect, the tracer velocity is obtained. The LDV is explained in detail in chapter 4 and the measurements and results are described in chapter 6. It came out that the flow profile at the nozzle exit is well shaped and the flow speed is in good agreement with the calculated flow Mach number M, i. e. M = 3.5, suitable for our future shock tunnel investigations.

For our shock tunnel operation it is desired to produce actual flow conditions around a projectile flying in earth atmosphere from ground level up to altitudes of more than 10 km with flight speeds up to 2000 m/s, i. e., Mach number $M \approx 6$. The Mach number M = 3.5 required in this study, was confirmed by the flow speed measurements using the ISL LDV system mentioned above. Additionally to the velocity measurements, the Pitot pressure, using a Pitot sensor, was registered and the required static gas pressure could also be confirmed.

1. Purpose of the study

For this study the ISL shock tube A has been used as a shock tunnel, i. e., at the end of the shock tube the flow is further accelerated inside a nozzle. For this purpose a divergent nozzle with a circular inner cone contour was designed and built. In this nozzle the supersonic shock tube flow is expanded up to the flow conditions desired. For our experimental applications the distribution of the longitudinal velocity $\vec{u}$ across the nozzle exit plane must be as homogeneous as possible for the required Mach number M = 3.5. This characterisation is an important factor for determining the quality of the nozzle used. Therefore, we measured the velocity profile at the nozzle exit cross-section with the LDV system developed by Smeets and George (1978) as well as the pressure distribution by measuring Pitot pressures.

2. Shock tube facility

In the ISL shock tube laboratory two high-pressure shock tubes , A and B, are operating since 1966 as described by Patz (1970, 1971). In Fig. 3 these two shock tubes can be seen looking towards the end of the shock tubes, i. e. the measuring sections. On the left hand side shock tube A and on the right shock tube B, having inner diameters of 100 mm, can be seen. The shock tubes are used to date as shock tunnels. They consist of a high pressure driver tube, a driven tube and a nozzle attached at its end as sketched in Fig. 1. A diaphragm separates the driver tube filled with H_2 or He and the driven tube containing the test gas which is either air (N_2 and O_2) or nitrogen (N_2). The driver gas fill pressure used is about 20 MPa to 60 MPa and the test gas fill pressure varies between 100 kPa and 600 kPa. After the diaphragm bursting, the driver gas expands into the driven tube, and a shock wave is produced inside of the driven tube accelerating the gas flow behind this shock wave to subsonic or supersonic flow speeds, depending on shock tube operation. In our case a supersonic shock tube flow is required which expands through the nozzle to the flow conditions required at the nozzle exit.

Fig. 3. View of shock tube laboratory

At the end of each shock tube a nozzle is attached, see e. g. in Fig. 4 a rectangular nozzle mounted at the end of tube B. The nozzle is fixed inside a test section which is attached at a dump tank for containing the driver and driven gases after shock tube firing. At both sides of the test section, optical windows are placed for flow diagnostics. Fig. 4 shows the nozzle exit through one of the opened windows. Here a square sectional nozzle is shown which was used at our laboratory for some decades. Using a rectangular nozzle cross-section results in some disadvantages, as the transition from circular shock tube section to square nozzle section and the boundary layer formation along each of the four inner nozzle corners. Fig. 5 shows a photograph of such a square test sectional nozzle. For the mentioned reasons the square nozzle outflow is not as homogeneous as desired. A square nozzle is only necessary in cases where a two-dimensional planar flow pattern must be present for flow investigations. Nowadays we use

circular models of flight vehicles mounted downstream of the nozzle exit. For such experiments a circular nozzle cross-section is more advantageous because it does not produce the distortions described above.
For the reasons discussed the new nozzle generation used in the ISL shock tube laboratory was manufactured with an inner circular cross-section and designed to be used as reflected shock tunnel nozzles as well as non-reflected nozzles. The operational mode, reflected or non-reflected, is the desired flow Mach number M. For M > 4.5 a nozzle with an inner throat contour is used with a shock reflection in front of the nozzle, i. e., reflected mode. But for Mach numbers M < 4.5 the throat cross section becomes too large and shock reflection is not longer well established. In this case the non-reflected mode must be applied with a nozzle whose throat cross section is equal to the diameter of the shock tube which is 100 mm. Therefore in this case the shock tube flow enters supersonically into the divergent nozzle attached at the end of the driven tube giving further flow acceleration.

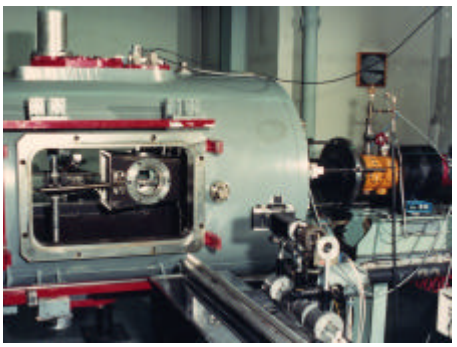

Fig. 4. Measuring section with nozzle

Fig. 5. Square cross-section nozzle

Because of the necessity of having a nozzle with the Mach number M = 3.5, a non-reflected working nozzle was designed, manufactured and investigated. A photograph of the nozzle is shown in Fig. 6 looking at the side of the nozzle exit. The inner nozzle shape is conical and the throat section is equal to the shock tube diameter, i. e. 100 mm. In Fig. 7 the inner part of the nozzle is visible showing the inflow section of 100 mm diameter as well as the outflow section with 250 mm diameter. A three-dimensional sketch is given in Fig. 8, showing the passage from the circular shock tube to the conical nozzle.

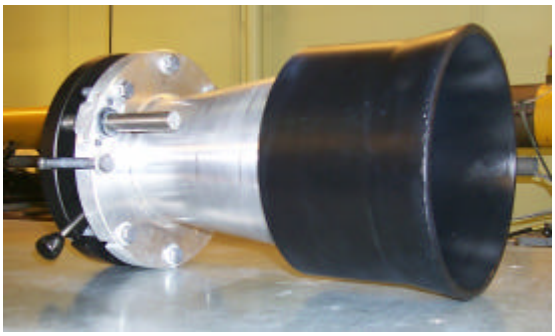

Fig. 6. Conical non-reflected nozzle

Fig. 7. Inner non-reflected nozzle shape

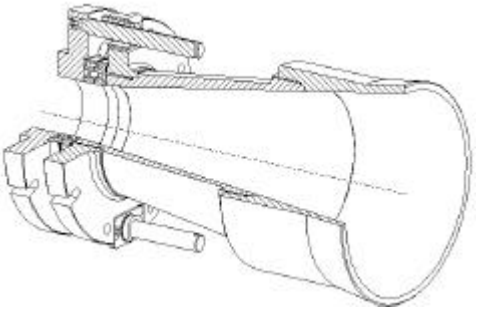

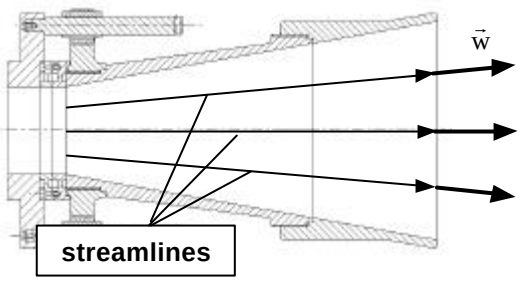

Fig. 8. Inner nozzle design *Fig. 9: Schematic of nozzle streamlines*

Fig. 9 shows a cross-section of the nozzle with some streamlines. Because of the conical nozzle shape with a 10° cone angle, the velocity vector $\vec{w}$ is off axis directed towards the nozzle walls with $\vec{w} = (u, v)$. The absolute amount of $|\vec{w}|$ is nearly constant across the exit cross-section, with $u = |\vec{w}| \cos\gamma$ and $v = |\vec{w}| \sin\gamma$, and streamline angle γ between 0° (axis) $\leq \gamma \leq$. 10° (wall).

In this study we are interested in the quality of our nozzle design with regard to the velocity profile of the axial flow speed u at the nozzle exit. Additionally some measurements have been done for detecting the Pitot pressure at the same locations as chosen for the LDV measurements. The Pitot pressure measurements have the aim of supporting the LDV investigations by looking for the expected pressure distribution across the exit cross-section as well.

3. Calculated flow conditions

The necessary flow conditions for shock tube operation have been calculated using Smeets's computer codes developed at ISL (1999) on the basis of the conservation equations of mass, momentum and energy together with the equations of state including real gas effects. With these codes the shock tube flow (2) and the expansion inside of the nozzle's exit (e) are calculated and the results are given in the following table for the LDV measuring plane placed 15 mm downstream of the nozzle exit. The driver conditions before diaphragm bursting are designated by (5), those in the driven tube by (1). With each of the shock tube experiments performed for this study, see table in chapter 6, an average shock speed $\dot{x}_S$ was determined and therewith the conditions (2) and (e) are calculated.

	conditions (1) test gas	conditions (5) driver gas	conditions (2)	conditions (e) 15 mm downstream
pressure p	280 kPa	20 MPa	2.97 MPa	110 kPa
density ρ	3.32 kg/ m^3		13.2 kg/m^3	1.235 kg/m^3
temperature T	293 K	293 K	777 K	313 K
velocity u			780 m/s	1255 m/s
sound speed a		743 m/s	550 m/s	355 m/s
Mach number M			1.43	3.53
shock speed $\dot{x}_S$			1040 m/s	

As driver gas we used a mixture of 87% hydrogen (H_2) and 13% nitrogen (N_2), the driven gas was air. The estimated test time is in the range of about 1.5 ms. Looking at conditions (e) we see that the flow conditions are in the range of the desired Mach number M = 3.5 at about ground level temperature and pressure conditions. These calculated design data, i. e., the flow velocity and gas pressure, have been checked by experiments carried out in the shock tunnel facility A of ISL using for flow velocity measurements the LDV (1978 – 1993) and for pressure measurements the special Pitot probes developed at the ISL shock tube laboratory.

4. Laser-Doppler-Velocimeter (LDV)

Velocity measurements for determining the longitudinal velocity distribution at the nozzle exit cross-section at different distances z from the centre line have been performed using the LDV developed by Smeets and George (1978). The experimental arrangement used is illustrated in Fig. 2. Monochromatic laser light from an Ar^+-laser (frequency ν_L) is transmitted by an optical fibre and focused by a lens on the measuring point downstream the nozzle exit cross-section. The Doppler-shifted light scattered by tracer particles (TiO_2) is collected by a second lens and transmitted via an optical fibre into the LDV. The LDV consists of a Michelson-Interferometer with different legs. The interferometer is sensitive to the frequency shift $d\nu$ of the scattered light with frequency ν_D caused by the Doppler effect and transforms the frequency shift $d\nu = (\nu_D - \nu_L)$ into a shift dI of the light intensity output I on the photomultipliers PH1 and PH2, see arrangement in Fig.10.

The working mechanism of the LDV can be understood in principle by discussing the optical arrangement depicted in Fig.10. After being linearly polarized by polarizer P1 by 45° (↗), the scattered light passes a Pockels cell PC and enters the Michelson-Interferometer. The 45° polarized scattered light vector (↗) is thought to be composed by two perpendicular polarized components (↗) = (→,↑). With the Pockels cell voltage U_{Pc} the phase difference $\Delta\varphi_{Pc}$ of both (→,↑) can be determined as

$$\Delta\varphi_{Pc} = k_{Pc}\, U_{Pc} \ . \tag{1}$$

The polarizing beam splitter cube SP1 separates the two incoming perpendicular polarized light beams (→,↑) of equal intensity on the mirrors M1 and M2, respectively. By means of a glass block placed in one of the two legs of the interferometer, an optical path difference $\Delta\phi$, i. e., a phase difference $\Delta\varphi$ is generated. The light intensity I in the image plane, given as light interference on the photomultipliers PH1 or PH2, depends on the phase difference $\Delta\varphi$ between the two legs and is as follows:

$$I = \hat{I}\cos^2\frac{\Delta\varphi}{2}. \tag{2}$$

The phase difference $\Delta\varphi$ is a function of the optical path difference $\Delta\phi$, the light source frequency ν_L and its speed of light c_0 measured in vacuum:

$$\frac{\Delta\varphi}{2\pi} = \nu_L\,\frac{\Delta\phi}{c_0} \ . \tag{3}$$

Differentiation of (3) with respect to $d\nu_L$ leads to the following expression, with $\lambda_0 = c_0/\nu_L$ being the light source vacuum wavelength:

$$d\left(\frac{\Delta\varphi}{2\pi}\right) = \frac{\Delta\phi}{\lambda_0}\,\frac{d\nu}{\nu_L} \ . \tag{4}$$

From relation (4) it can be withdrawn that frequency changes $d\nu$ cause changes $d(\Delta\varphi)$ of $\Delta\varphi$ between the light beams of the two legs and also cause changes of light intensity I by dI.

After leaving the Michelson-Interferometer, the two beam parts of both legs (→,↑) pass a second polarising beam splitter SP2 with its optical axis turned by 45° with regard to the directions of (→,↑). Each of these two perpendicular polarized beams (→,↑) is splitted into two parts, (→) = (↗,↘) and (↑) = (↖,↗), which interfere complementary at the two photomultipliers (or photodiodes) PH1 and PH2 used for output registration:

$$\text{PH1: } I_1 = \hat{I}_1\cos^2\frac{\Delta\varphi}{2} \ , (\nearrow,\nearrow) \tag{5a}$$

$$\text{PH2: } I_2 = \hat{I}_2\sin^2\frac{\Delta\varphi}{2} \ , (\searrow,\nwarrow). \tag{5b}$$

The photomultiplier currents i_1 and i_2 of PH1 and PH2, respectively, are proportional to the light intensity I_1 and I_2, respectively, and are given as:

$$i_1 = k_1\, I_1 \text{ and } i_2 = k_2\, I_2 \ . \tag{6}$$

A change in the frequency ν_D of the scattered light, i. e., $d\nu = (\nu_D - \nu_L)$, leads as discussed to a phase change $d(\Delta\varphi)$ followed by a complementary light intensity variation at the two photomultipliers PH1 and PH2. As I_1 is complementary to I_2, the currents i_1 and i_2 are also complementary to each other. Both are subtracted, $(i_1 - i_2)$, by using a circuitry as shown in principle in Fig. 10 with a capacitor C placed as electrical "bridge" between the photomultipliers PH1 and PH2:

$$i_1 - i_2 = k\hat{I}\left(\cos^2\frac{\Delta\varphi}{2} - \sin^2\frac{\Delta\varphi}{2}\right) = k\hat{I}\cos\Delta\varphi \ , \text{ with } k_1 = k_2 = k = \text{constant}. \tag{7}$$

The initial condition with $d\nu = 0$ is that $(i_1 - i_2) = 0$, i. e., the Michelson-Interferometer is adjusted to

$$\Delta\varphi = \frac{\pi}{2} \pm n\pi,\ n = 0, 2, 4, \ldots \tag{8}$$

with $I_1 = \hat{I}_1/2$, $I_2 = \hat{I}_2/2$ and $i_1 = i_2$. As ν_D changes by the Doppler effect versus time t by $d\nu$, $\Delta\varphi$ changes by $d(\Delta\varphi)$. see equation (4). Both currents i_1 and i_2 develop complementary with $di_1 = -di_2$ causing a compensating capacitor bridge current $(i_1 - i_2) \neq 0$.

The capacitor voltage change $U_C(t)$ is given as

$$U_C(t)=\frac{Q(t)}{C}\ , \tag{9}$$

with

$$Q=\int_{t=0}^{t}(i_1-i_2)\,dt\ . \tag{10}$$

U_C (t) is used as feedback voltage to instantaneously shift back the phase change d(Δφ), see equation (4), by an equal Pockels cell phase change

$$d(\Delta\varphi_{Pc})=-d(\Delta\varphi)\,. \tag{11}$$

As a result, the phase change d(Δφ) given by frequency change dν is automatically compensated within the Pockels cell PC by a response time of less than one microsecond.

Since the (i_1-i_2) change, i. e., the $U_C(t)$ change, is practically linearly depending on the phase change d(Δφ) for small d(Δφ), and since the Pockels effect is linear, the Pockels cell voltage change

$$dU_C=U_C(t)-U_0\,, \tag{12}$$

is proportional to the frequency shift dν, caused by the Doppler-effect. The Pockels cell voltage history is therefore directly proportional via a calibration to the frequency change caused by the tracers passing the measuring point. The complementary light intensity registration by PH1 and PH2, together with the bridge circuitry of Fig. 10 makes the output signal $U_C(t)$ independent of varying light intensities $d\hat{I}=d\hat{I}_1=d\hat{I}_2$ given by inhomogeneously distributed tracer particles in gas flows. Changes of $d\hat{I}$ influence both currents i_1 and i_2, respectively, in the same manner and therefore do not affecting the difference $(i_1 - i_2)$, but only at $(i_1 - i_2) = 0$ at the phase condition (8). Nowadays, a special analogue signal processing device is used for signal processing. This electrical circuitry, see Fig. 11, works in principle as discussed above, but normalises the $(i_1 - i_2)$ current by its sum $(i_1 + i_2)$:

$$\frac{i_1-i_2}{i_1+i_2}=\cos\Delta\varphi\ . \tag{13}$$

Thereby the intensity changes $d\hat{I}$ are better compensated as using only $(i_1 - i_2)$:

$$U_C(t)=\frac{i_{ref}}{C}\int_{t=0}^{t}\frac{i_1-i_2}{i_1+i_2}dt+U_0\ . \tag{14}$$

U_0 is used for LDV control purposes giving a $(\Delta\varphi_{Pc})_0=k_{Pc}\,U_0$. The current i_{ref} is a reference value determined by the processing system shown in Fig. 11.

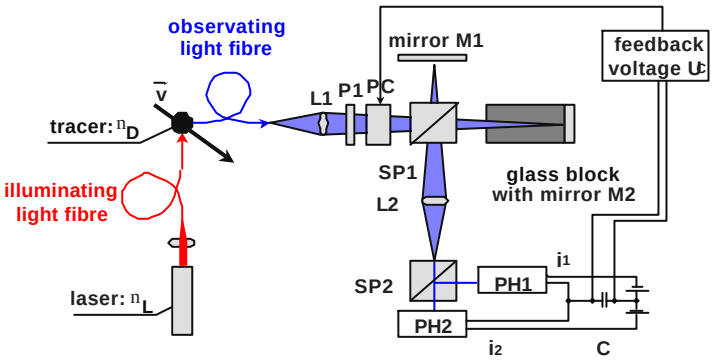

Fig. 10. LDV system

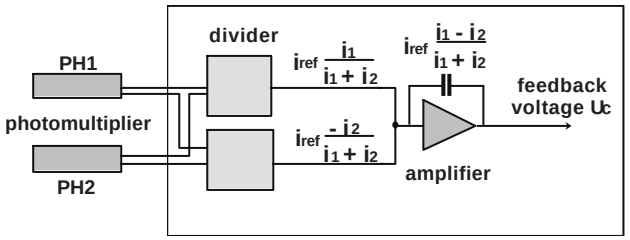

Fig. 11. Principle of processing circuit

The well-known classical laser anemometry theory is used to determine the flow speed v depending on the frequency shift $d\nu = \nu_D - \nu_L$ based on the Doppler effect as given in relation (15). The vector diagram in Fig. 12 describes the vectors $\vec{e}_D$ and $\vec{e}_L$ as well as the angles γ and θ.

$$\frac{\nu_D - \nu_L}{\nu_L} = \frac{\vec{v}\left(\vec{e}_D - \vec{e}_L\right)}{c} = 2\frac{v}{c}\cos\gamma \sin\frac{\theta}{2} \quad . \qquad (15)$$

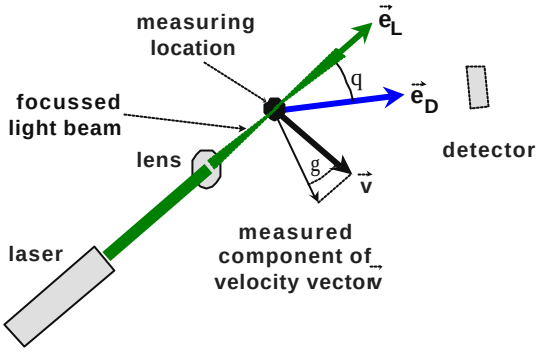

Fig. 12. Doppler effect

6. Velocity contour results

The time history of the velocity distribution was measured with the LDV 15 mm downstream from the nozzle exit at different measuring locations, i.e., distances z from the nozzle axis. These locations together with the shock tube firing numbers are given in the following table:

location z/mm	- 105	- 62	- 20	0	20	62	105
shock tube firing number of series A2	990826.01	990826.02	990826.03	990825.01 990825.02 990826.04 990830.01	990830.02	990830.03	990831.01

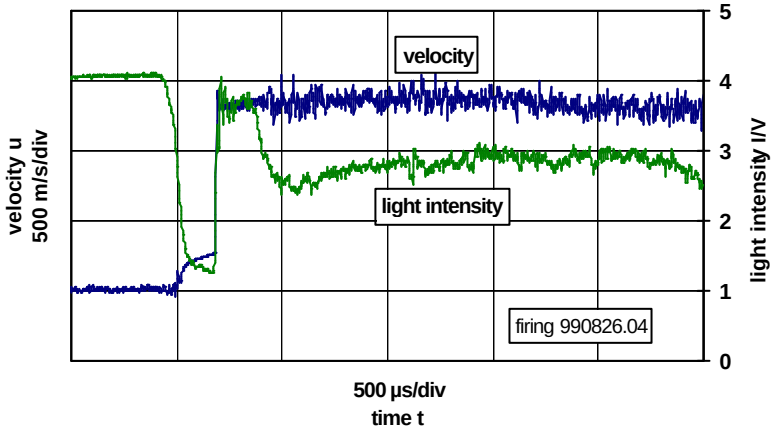

Fig. 13. Time history of the LDV output for z = 0

Fig. 13 shows the intensity of the scattered light and the velocity variation at z = 0 mm and x = 15 mm for the experiment no 990826.04. TiO_2 tracer particles are used and are entrained into the shock tube air test gas via a specially developed particle seeding system. For having at the beginning of the velocity recording the line for zero flow velocity, i. e., for no Doppler shift, the illuminating light beam is directly turned via a mirror and a light fibre into

the Michelson-Interferometer, see Fig. 14. This means that the light intensity signal in Fig. 13 starts at a certain level depending on the diminution of the directly captured laser light. The light frequency is not shifted and the speed output is zero. Then, shortly before flow onset the mirror is suddenly turned by an electromagnet and the light coming from the Ar^+-laser (power = 1.5 W) is focussed on the measuring point. The time difference from mirror turning up to the flow onset here is about 200 µs depending on the trigger time point for turning the mirror. During this time interval no tracer particles are available and therefore no scattered light enters the Michelson-Interferometer. The light intensity is nearly zero and the velocity drifts to a certain adjustment value. With flow onset, tracer particles are crossing the measuring point and the intensity of the scattered light immediately increases followed by a Michelson-Interferometer voltage output representing the velocity distribution versus time. By a calibration factor this voltage output is transformed into the flow speed distribution shown in Fig. 13

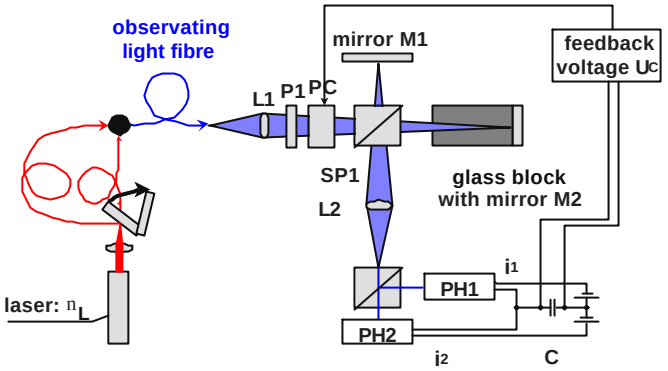

Fig. 14. Initiation of the LDV

Looking at the development of the light intensity distribution in Fig. 13, we see that it needs enough light intensity I for the LDV system to start its measuring cycle. The illumination on the photomultipliers increases and from a certain level of illumination, about 2 volts, the LDV begins working. The starting process lasts until the required amount of particles per volume is available for having enough scattered light intensity. This process is dominated by the inertia of the particles, i. e., the slip between particles and flow onset. Therefore the flow start cannot be determined from the velocity distribution shown in Fig. 13. By stepwise varying the horizontal measuring location z from z = - 105 mm up to z = 105 mm the following velocity distributions have been obtained: z = - 105 mm (Fig. 15), - 62 mm (Fig. 16), - 20 mm (Fig. 17), 20 mm (Fig. 18), 62 mm (Fig. 19) and 105 mm (Fig. 20).

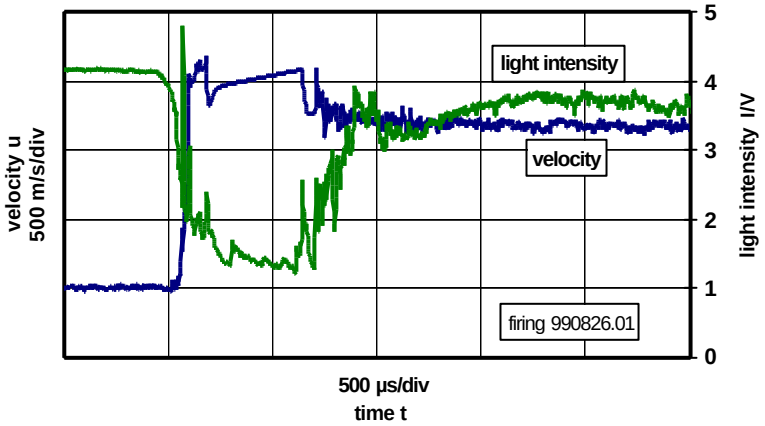

Fig. 15. Time history of the LDV output for z = - 105 mm

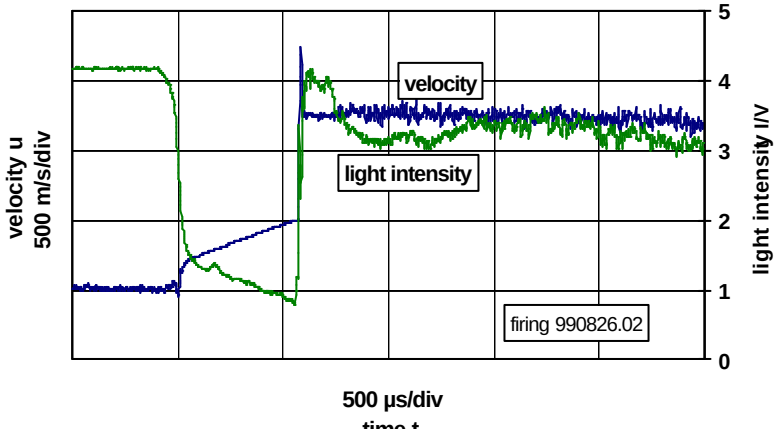

Fig. 16. Time history of the LDV output for z = - 62 mm

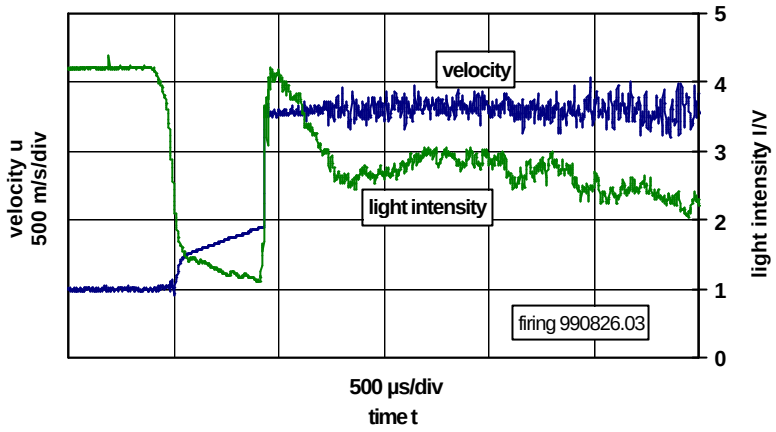

Fig. 17. Time history of the LDV output for z = - 20 mm

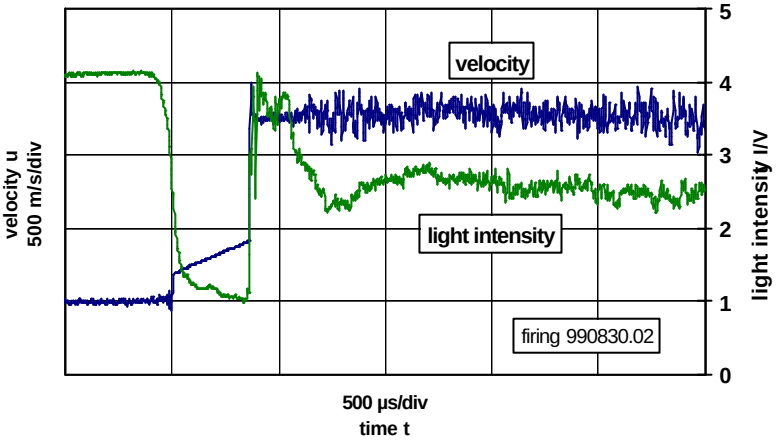

Fig. 18. Time history of the LDV output for z = 20 mm

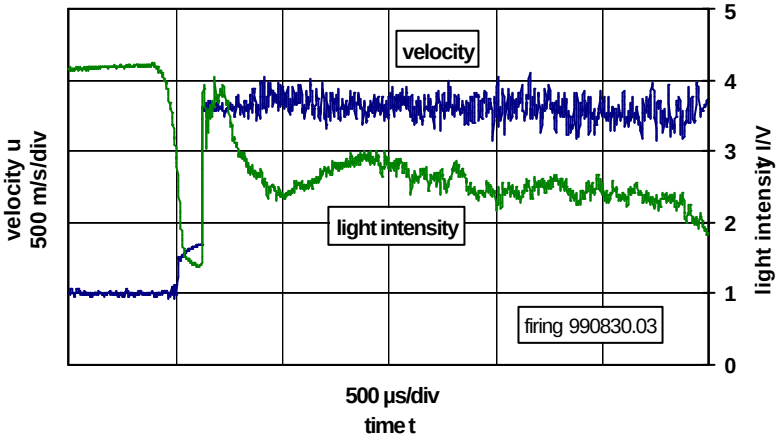

Fig. 19. Time history of the LDV output for z = 62 mm

The result of the velocity diagnostic is that after a certain flow starting time of some hundreds of microseconds the flow velocity at the nozzle exit becomes nearly constant for a test time of about 1.5 ms, see Fig.15 up to Fig. 20. This outcome is depicted in Fig. 21a with the measured velocities (dots), showing the mean value of the velocity level present during these 1.5 ms. The velocity cross-section contour was fitted with an exponential curve profile. Close to the axis this velocity distribution is nearly constant with u = 1285 m/s, as desired for our experimental purposes. Towards the nozzle wall the influence of the boundary layer becomes noticeable followed by the expected velocity decrease. In Fig. 21b the speed values calculated without boundary layer are included for each shock tube firing. These calculated velocity data are fitted, resulting in a flow speed of u = 1255 m/s with M = 3.5. The deviation between experiment and calculation

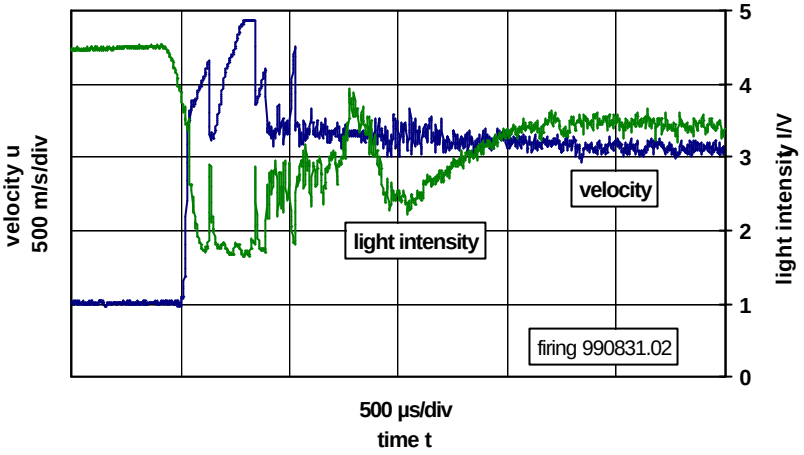

Fig. 20. Time history of the LDV output for z = 105 mm

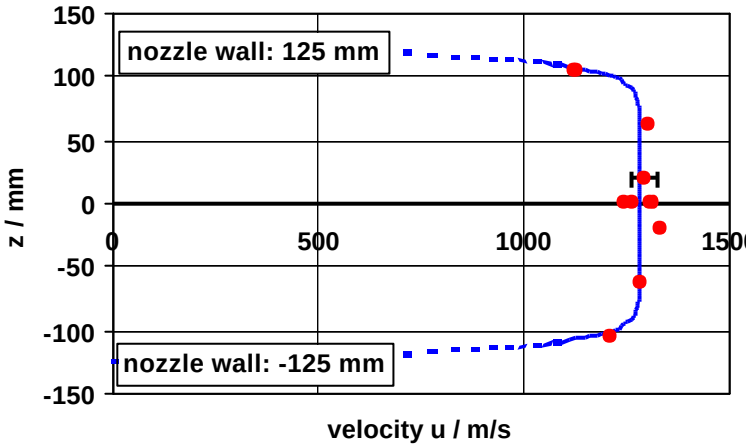

Fig. 21a. Experimental velocity contour at the exit of the nozzle

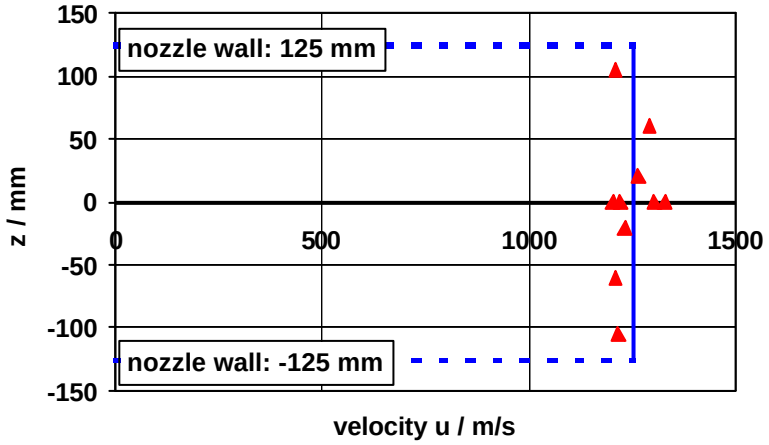

Fig. 21b. Calculated velocity contour at the exit of the nozzle

7. Pitot pressure

Additionally to the flow velocity measurements described in chapter 6, Pitot pressure measurements have been performed at the exit of the nozzle in a distance of 10 mm downstream of the exit cross section. The shock tube firing conditions are calculated as explained in chapter 3 using the computer codes of Smeets (1999) and are practically identical to those given in the table of chapter 3. The Pitot pressure (or total pressure) is given as the static pressure plus kinetic energy per volume. For calculating the Pitot probe pressure in supersonic flow the Rayleigh supersonic Pitot-tube formula has to be taken into account. Using Smeets's codes a Pitot pressure of p_{Pitot} = 1.63 MPa was calculated for the average shock tube firing conditions given in chapter 3.

The measuring locations are practically identical as for the velocity measurements, see chapter 6: z = - 105, - 62, -21, 21, 62, 105 mm. The measured Pitot pressure distributions are depicted in Fig. 22 versus measuring time. In the core flow at z = - 62, -21, 21, 62 mm the measured and calculated Pitot pressure data agree well within a deviation of some percent. At z = - 105 and 105 mm the nozzle boundary layer influences the flow in a velocity decrease, see Fig. 21, and consequently a Pitot pressure drop.

7. Conclusions

A new conical nozzle was designed for ISL shock tunnel A, manufactured and tested for experimental applications. With the Laser-Doppler-Velocimeter (LDV) developed by Smeets and George (1978) the flow velocity was measured 15 mm downstream of the nozzle exit and at radii z = - 105, - 62, -20, 0, 20, 62, 105 mm. The experimental results are compared with calculated speed data showing small deviations from each other. From Fig. 21 we see that the mean velocity profile in the core flow is nearly flat for z = ± 90 mm. This region is suitable for our experimental investigations. Outside this test core the boundary layer mixing decreases the flow velocity and this flow part should not be used for experimental purposes. Furthermore, Pitot pressure measurements show also good agreement with the calculation, resulting from Smeets codes (1999) supporting the above mentioned outcome about the quality of the nozzle and its application for future shock tunnel experiments. From the Pitot pressure signals in Fig. 22 the nozzle starting time is about 500 µs followed by a test time of about 1.5 ms with a nearly constant pressure plateau which ranges between $1.5 < p_{Pitot} < 1.8$ Mpa.

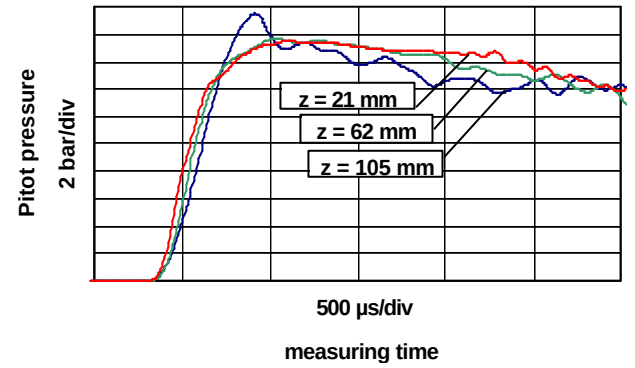

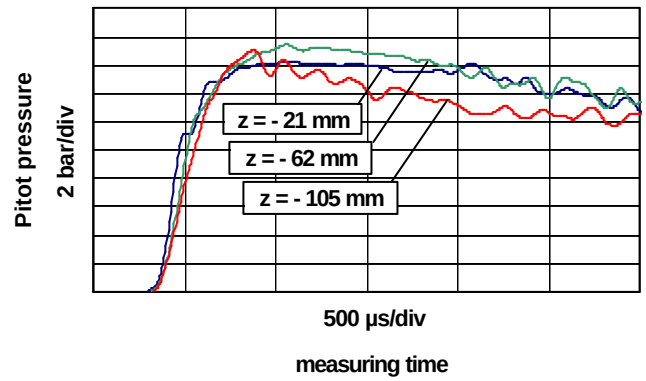

Fig. 22. Pitot pressure distribution
at 10 mm from the nozzle's exit
(experiment A2/990722.01)

An extensive list of literature describing the Laser-Doppler-Velocimeter is given in the references for papers published by Smeets et al. (1978 up to 1993), as well as for some applications published by Srulijes (1989) and Seiler (1989 up to 1992). An extensive description of the shock tube laboratory design is found in the reports of Patz (1970, 1971).

References

Patz, G. (1970). "Das Hyperschallstoßrohrlabor des ISL, 3. Teil: Stoßrohr B", ISL-Report N 30/70

Patz, G. (1971). "Das Hyperschallstoßrohrlabor des ISL, 2. Teil: Stoßrohr A", ISL-Report N 27/71

Smeets, G. and George, A. (1978). "Instantaneous laser Doppler velocimeter using a fast wavelength tracking Michelson interferometer", Review of Scientific Instruments, 49(11)

Smeets, G. and George, A. (1979). "Novel Laser-Doppler-Velocimeter enabling fast instantaneous recording", ISL-Report CO 212/79

Smeets, G. and George, A. (1981). "Michelson spectrometer for instantaneous Doppler velocity measurements", Journal of Physics E: Scientific Instruments, Vol. 14, pp. 838-845

Smeets, G. (1982). "Laser Doppler velocimetry with a Michelson spectrometer", International Symposium on Applications of Laser-Doppler Anemometry to Fluid Mechanics, Lisbon, Portugal, 1982 and ISL-Report CO 210/82

Smeets, G., George, A. and Mathieu, G. (1982). "Laser-Interferenz-Velozimeter. Anwendungen am Brennerstrahl", ISL-Report N 604/82

Smeets, G. and Mathieu, G. (1987). "Velocity interferometry in shock tubes and shock tunnels", ISL-Report CO 203/87

Smeets, G. (1988). "Interferometrische Geschwindigkeitsmessungen", ISL-Report CO 221/88

Srulijes, J., Seiler, F. and Smeets, G. (1989). "Laser-Doppler-velocimeter measurements of shock- and piston induced turbulent boundary layer in a shock tube", Proceedings of the 3rd International Conference of Laser Anemometry, Advances and Applications, Swansea, U.K., and ISL-Report CO 227/89

Seiler, F. (1989). "Velocity measurements in piston-induced turbulent boundary layers in a shock tube", Proceedings of the 13th International Congress on Instrumentation in Aerospace Simulation Facilities Record, IEEE Publication, New York, USA, and ISL-Report CO 235/89

Seiler, F., George, A., Mathieu, G. and Smeets, G. (1990). "The Laser-Doppler-Velocimeter for Flow Diagnostics: Density and Velocity Measurements in Post-Piston Boundary Layer Flow", Proceedings of the 5th International Symposium on Applications of Laser Anemometry to Fluid Mechanics, Lissabon, Portugal, and ISL-Report CO 208/90

Seiler, F., Srulijes, J. and Mathieu, G. (1990). "Nichtideales Verhalten der Laufgasströmung in einem Stoßrohr unter Einfluß der turbulenten Stoßgrenzschicht", ISL-CO 213/90

Seiler, F. and Mathieu, G. (1991). “Velocity measurements in piston-induced turbulent boundary layers in a shock tube”, Laser Anemometry, Advances and Applications, ASME Publication, New York, and ISL-Report CO 211/91

Smeets, G. and George, A. (1992). “Simple experiments for testing and calibrating the ISL laser Doppler velocimeter”, ISL-Report R 124/92

Smeets, G. (1993). “Doppler Velocity Measurements Using a Phase Stabilized Michelson Spectrometer”, International Symposium on Non-Intrusive Combustion Diagnostics, Scheveningen, Netherlands, and ISL-Report PU 314/93

Smeets, G. (1999). “Computer Codes at ISL”